SECURITY CLASSIFICATION OF THIS PAGE

(4)

REPORT DOCUMENTATION PAGE

1a REPORT SECURITY CLASSIFICATION: Unclassified/Unlimited	1b. RESTRICTIVE MARKINGS
	DISTRIBUTION / AVAILABILITY OF REPORT: Approved for Public Release Distribution Unlimited
AD-A212 595	
4 PERFORMING ORGANIZATION REPORT NUMBER(S): Number 1	5. MONITORING ORGANIZATION REPORT NUMBER(S): N00014-89-J-1197
6a NAME OF PERFORMING ORGANIZATION: Stanford University; 6b OFFICE SYMBOL (If applicable)	7a. NAME OF MONITORING ORGANIZATION: Office of Naval Research, Dr. R. Schwartz
6c ADDRESS (City, State, and ZIP Code): Mechanical Engineering Dept., Bldg. 520, Stanford, CA 94305-3032	7b. ADDRESS (City, State, and ZIP Code): Code 3854, Naval Weapons Center, China Lake, CA 93555
8a. NAME OF FUNDING / SPONSORING ORGANIZATION; 8b. OFFICE SYMBOL (If applicable)	9. PROCUREMENT INSTRUMENT IDENTIFICATION NUMBER
8c. ADDRESS (City, State, and ZIP Code)	10 SOURCE OF FUNDING NUMBERS: PROGRAM ELEMENT NO. / PROJECT NO. / TASK NO / WORK UNIT NO

11 TITLE (Include Security Classification)

An Investigation of Diamond Film Deposition in a Premixed Oxyacetylene Flame

12 PERSONAL AUTHOR(S)

M. A. Cappelli and P. H. Paul

13a. TYPE OF REPORT	13b. TIME COVERED	14 DATE OF REPORT (Year, Month, Day)	15. PAGE COUNT
Technical	FROM _____ TO _____	1989, September, 10	25

16 SUPPLEMENTARY NOTATION

Submitted to Journal of Applied Physics

17 COSATI CODES			18. SUBJECT TERMS (Continue on reverse if necessary and identify by block number)
FIELD	GROUP	SUB-GROUP	Flame Deposition, Diamond Synthesis, Laser Induced Fluorescence Diagnostics

19 ABSTRACT (Continue on reverse if necessary and identify by block number)

Diamond film has been deposited in a single-nozzle pre-mixed oxy-acetylene flame. Results of runs of varying duration suggest that diamond is deposited via the transport of hydrocarbon fragments produced at the secondary flame front. *Planar laser induced photodissociation fluorescence* suggests that this region is rich in C_2H species. Emission studies also suggest that the post primary flame zone presents a source of C_2 radicals which may account for the observed graphite and diamond-like carbon deposited on the substrate exposed to this region of the flame. The results on the pre-mixed flame suggest that it would be possible and more convenient to attempt large area deposition using a multi-nozzle diffusion flame.

20 DISTRIBUTION / AVAILABILITY OF ABSTRACT: ☐ UNCLASSIFIED/UNLIMITED ☒ SAME AS RPT. ☐ DTIC USERS	21 ABSTRACT SECURITY CLASSIFICATION
22a NAME OF RESPONSIBLE INDIVIDUAL	22b TELEPHONE (Include Area Code); 22c. OFFICE SYMBOL

OFFICE OF NAVAL RESEARCH

Contract N00014-89-J-1197

Task No. 431A022

TECHNICAL REPORT NO. 1

AN INVESTIGATION OF DIAMOND FILM DEPOSITION IN A PREMIXED OXYACETYLENE FLAME

Submitted by

Mark A. Cappelli and P. H. Paul

Stanford University
Mechanical Engineering
High Temperature Gasdynamics Laboratory
Stanford, CA 94045-3032

September 11, 1989

HIGH TEMPERATURE GASDYNAMICS LABORATORY
Mechanical Engineering Department
Stanford University

AN INVESTIGATION OF DIAMOND FILM DEPOSITION IN A PREMIXED OXYACETYLENE FLAME

M. A. Cappelli and P. H. Paul

High Temperature Gasdynamics Laboratory
Stanford University,
Stanford California, 94305-3032

ABSTRACT

Diamond film has been deposited in a single-nozzle premixed oxyacetylene flame. Results of runs of varying duration suggest that diamond is deposited via the transport of hydrocarbon fragments produced at the secondary flame front. *Planar laser-induced photodissociation fluorescence* suggests that this region is rich in C_2H species. Emission studies also suggest that the post primary flame zone presents a source of C_2 radicals which may account for the observed graphite and diamond-like carbon deposited on the substrate exposed to this region of the flame. The results on the premixed flame suggest that it would be possible and more convenient to attempt large area deposition using a multi-nozzle diffusion flame.

I. INTRODUCTION

Polycrystalline diamond film synthesis has been demonstrated using a wide variety of enhanced chemical vapor deposition (CVD) techniques. These are best described in a recent review article by Spear[1]. The method of choice depends on the end application of the deposited film or coating. Low pressure (< 50 torr) plasma enhanced CVD shows great promise for large area deposition and better control of film properties in that one can have independent control over the plasma source (radical pool) and substrate temperature. The growth rates for low pressure plasma enhanced CVD are typically 1-3 μm/hr and increase slightly upon the addition of oxygen[2]. High pressure CVD techniques such as thermal plasma[3] and flame synthesis[4-7] have considerably higher growth rates (typically >> 10 μm/hr) but have the drawback that the reactive gas stream is also responsible for a considerable heat flux to the substrate as well as the growing diamond film. It has been observed that diamond films of reasonable quality generally grow within a narrow surface temperature range (600 - 900 °C)[1]. As a result, the deposit morphology obtained using such high growth rate sources in some way reflects the temperature profile of the high enthalpy stream. In addition, it has been shown recently that diamond deposition in premixed oxyacetylene flames occurs primarily at the secondary flame boundary[4]. This suggests that even if the heat transfer problem were indeed solved, one is confronted with a perhaps greater problem in designing a more uniform source of reactive species.

In the premixed oxyacetylene flame synthesis of diamond at atmospheric pressure, the optimum results are obtained when the torch is operated fuel rich. The flame appears to have the familiar primary flame front resulting from the reaction of the oxygen and acetylene feed gas mixture (Figure 1). The majority of the heat generated by the flame originates in this reaction zone. The excess acetylene is consumed some distance downstream by reaction with entrained oxygen from the surrounding room air. The region where this reaction takes place defines the secondary (diffusion) flame front. The surprising fact that diamond is found to grow in an annular region determined by the intersection of this secondary flame with the substrate, suggests that the source of radicals responsible for diamond growth originate as intermediates of the secondary flame reaction. Although the region between the primary and secondary flame (post-primary flame zone) is expected to be rich in acetylene, the atomic hydrogen and smaller hydrocarbon fragment concentrations are expected to be low (mole fractions less than 10^{-4}), and the area of the substrate in contact with this region (referred to in this paper as the central region) is found to contain non-diamond carbon[5].

These observations are in some ways consistent with the mechanism proposed by Frenklach and colleagues[8,9] which suggests that diamond growth proceeds via the transport of gas phase monomers (condensate) of the type C_2H_x to the surface and is

mediated by the action of atomic hydrogen. Atomic hydrogen is believed to play a paramount role in creating the active site for incorporation of the monomer into the lattice, as well as in the efficient etching (removal) of non-sp^3 bonded carbon. In the central region of the deposit, the absence of diamond and the presence of non-diamond carbon might then be explained by the absence of sufficient levels of atomic hydrogen. In the annular region where diamond is prevalent, it is possible that the OH radical and atomic oxygen play a similar role to that proposed for atomic hydrogen[8] (i.e., hydrogen abstraction and graphite etching) since the concentration of OH and O within the secondary flame sheet can be significantly increased through chain reactions with O_2, H and H_2O[10]. The rapid production of OH within the secondary flame zone should be accompanied by the rapid consumption of acetylene. If both acetylene and OH are required for diamond growth, then they may be simultaneously present at sufficient quantities only within a narrow spatial region within the secondary flame sheet. This might account for the annular ring-like deposit observed by others[4] and also described in this work. Alternatively, it is conceivable that reactive radical intermediates (produced early in the combustion of acetylene within the secondary flame zone) such as C_2H act as the dominant growth species. In this paper, we report on the use of in-situ planar laser-induced fluorescence and emission spectroscopy as a diagnostic tool for visualizing the C_2H radical and C_2 molecule distribution within the vicinity of the substrate surface during diamond deposition on silicon.

II. EXPERIMENT

A. Flame Deposition Facility

The premixed oxyacetylene flame deposition facility consisted primarily of a standard brazing torch fitted with a number one tip. Gas flow to the torch was controlled using calibrated rotometers. The silicon wafer substrates (100) were scratched with 6 μm diamond paste, rinsed and bathed in ethanol, then mounted on a water cooled stainless steel block. A thermocouple probe was used to monitor the temperature of the block surface just below the silicon wafer. A disappearing filament pyrometer was used to measure the brightness temperature (at 655 nm) of the substrate surface. Experiments under conditions of varying the oxygen to acetylene volumetric flow ratio (R) and nozzle-substrate separation (D) from the surface were performed. The results were qualitatively similar to that reported by Hanssen et al.[4] in that well faceted crystals were found to grow primarily in an annular ring where the secondary flame boundary intersected the silicon substrate. The growth rate and morphology were found to be sensitive to R (between 0.6 and 1.4) and surface temperature (800 - 1200 °C). Optimum results were obtained for short duration runs (< 15 minutes) with R = 0.9, D= 1.1cm and

a surface temperature near the center of the substrate deposition region of approximately 900° C. At the optimum conditions, only well faceted crystals were found to grow within an annular region approximately 4 mm in diameter. Here, we report only on a series of experiments performed under these conditions of flow ratios, nozzle-substrate separations and surface temperatures. The reader is referred to the work of Hanssen et al[4]. for the results of a more detailed parametric study as to the effects of these process parameters on the deposit morphology.

B. Laser and Emission Diagnostics Facility

In order to better understand the role of gas phase precursors to diamond deposition, we have undertaken spatially resolved instantaneous measurements of laser-induced fluorescence from what we believe is the relative ground state C_2H radical distribution within the flame. This work is an extension of research in our laboratory by Hanson and colleagues[11], that has involved the development of planar laser induced fluorescence (PLIF) techniques for the two dimensional visualization of radical species within flames.

A schematic of the laser based diagnostic facility is presented as Figure 2. The output laser beam from an ArF excimer laser (Lambda-Physik model EMG150T-MSC) at 193.0 nm is optically shaped into a sheet (cross-section dimension: 2 cm x 100 μm) that bisects the flame through the central axis of symmetry. The laser beam energy is typically 100 mJ, with a temporal pulse width of approximately 15 ns and is operated at 30 Hz. This radiation is believed to interact primarily with C_2H through a single photon transition[12] and C_2H_2 through a two-photon transition[13,14]. Both processes leave the species in highly excited states which rapidly dissociate, producing the electronically excited $CH(^2A\Delta)$ radical directly (in the case of acetylene absorption), or indirectly (in the case of C_2H) through the production of $C_2(^3\Pi_u)$[12] which subsequently reacts with the OH ($^2\Pi$) radical to produce $CH(^2A\Delta)$[15,16]. The pumping strategy for this study is illustrated in Figure 3. Radiative decay down to the $CH(^2X\Pi)$ state at approximately 431 nm can be observed at right angles to the laser beam direction with an image intensified CCD camera. The camera is gated so as to accept fluorescence over a 1 μs interval commencing with the onset of the laser pulse. Frames corresponding to individual laser shots are handled by appropriate electronic hardware and stored on a laboratory computer. The fluorescence is spectrally discriminated from background and interfering transitions by use of narrow band (10 nm) interference filters.

III. EXPERIMENTAL RESULTS

A. Growth Morphology

Photographs of the full deposit region (taken through an optical microscope at low magnification) for run durations of 5 and 30 minutes are shown in Figures 4a) and 4b) respectively. Also shown in the figures are magnified fields of positions near the outer edge of the deposition region. Short duration runs (< 30 min) clearly show a deposit primarily in an annular region. The crystals in this region are well faceted, as seen under a scanning electron microscope (SEM), where as the crystallites within the central region are spherical in shape. The onset of nucleation within the central region is found to be longer than that in the annular region, however, growth of non-diamond carbon in this central region proceeds quickly so as to form a dense continuous film between 30 minutes and one hour. It is further observed that the well faceted crystallites in the annular region (for short growth periods) grow into spherillites comprised predominantly of graphite after approximately one hour. Scanning electron micrographs (Figure 5) and Raman analysis (Figure 6) of the two regions (central and annular) for the 30 minute run confirms that the central region is predominantly graphitic and perhaps diamond-like carbon in phase, whereas the annular deposit depicts the characteristic 1332 cm^{-1} shift associated with diamond.

The existence of the annular ring in which diamond growth persists can be in part explained by the existence of a radially decreasing temperature field. Within the central region, one might postulate the temperature to be too high for diamond growth, (approximately 1000 °C as estimated by the pyrometer) leading to graphite growth at the surface, whereas outside the annular disk, the temperature is too low to support carbon condensation, based on thermodynamic calculations. We found however that the radius of the annular disk is relatively insensitive to the peak (center) temperature. Instead, we found a stronger correlation between the location of the annular region and the position of the secondary flame (determined by laser-induced fluorescence of C_2H radicals as described below). This suggests that the morphology is more likely driven by the reactive species transport from the gas phase.

B. Fluorescence and Flame Emission

Figure 7 shows the two-dimensional map of fluorescence centered around 431 nm, arising from what is interpreted as direct excitation of a C_2H radical in the electronic ground state. Examination of fluorescence within a bandwidth centered about 510 nm (in the vicinity of the $d^3\Pi_g$-$a^3\Pi_u$ transition in C_2) shows negligible production of excited C_2 and reinforces our assignment of the 431 nm emission to the $^2\Delta$-$^2\Pi$ transition in CH. The absence of fluorescence from the central region of the flame (post-primary flame zone) indicates that two-photon excitation and photodissociation of acetylene, expected to be

present in this region in large quantities (see Discussion below), is negligible. The fluorescence is interpreted as reflecting the annular distribution of C_2H radicals produced within the secondary flame zone. The bright bar at the top of the image represents the location of the surface relative to the fluorescence. The dark region between the surface and fluorescence is a result of the fact that the laser sheet passes through the flame at approximately 1 mm below the surface. Closer inspection of the numerical data parallel to, and approximately 1 mm below the surface (Figure 8) indicates that the fluorescing species occupy an annular region near the substrate and qualitatively, correlates very well to the region on the substrate where well facetted crystals are found to grow.

Figure 9 shows the two dimensional (path averaged) image of the intrinsic CH emission (CH signal at 431 nm in the absence of the 193 nm laser). The intensity is found to peak along the axis of symmetry immediately below the substrate surface. It is well known that intrinsic emission from flames is the result of chemiluminescent reactions between flame radicals. As mentioned earlier, there is experimental evidence[15,16] suggesting that CH chemiluminescence at 431 nm arises primarily from the chemical reaction between C_2 and OH:

$$C_2(a^3\Pi_u) + OH(^2\Pi) \rightarrow CO(^1\Sigma) + CH(^2\Delta) \ ,$$

in which case, the relative intensity of the CH chemiluminescence reflects regions rich in either C_2 or OH reactants. It is counterintuitive to expect the highly reactive OH radical mole fraction to increase approaching the cooler surface, thus the increased emission is more likely explained by a sudden increase in molecular carbon. These emission data are weakly supportive of the conjecture[17] that C_2 rich reactive streams may be responsible for preferential graphite or diamond-like carbon growth regularly observed in the central region of the deposit. If this mechanism of $CH(^2A\Delta)$ formation is indeed correct, then the relative CH emission signal may be an indicator of relative C_2 species concentration and can be a potentially useful tool in a more detailed parametric study.

C. Extended Growth

We have found that the crystals in the annular region eventually lose their facetted structure during extended growth (longer than 30 min), and proceed to grow into the spherical structure that is predominant in the central region. Assuming that the gas phase chemistry and transport remains constant, then this could only be explained by way of a change in the surface kinetics. All else being equal, the surface kinetics is controlled by the surface temperature. The temperature of the surface of a growing crystal is determined by the balance between the net heat conducted to the surface by the adjacent gas layer and the loss of heat from the surface through radiation to its environment and conduction to the underlying substrate (Figure 11). In a simplified form, this balance can be expressed as

$$k_{SiC} A_{SiC} (T_{Di}-T_S)/\Delta X_{SiC} + \varepsilon_{Di} \sigma T^4_{Di} A_{Di} = Q_{conv} A_{Di}$$

Here, k_{SiC}, A_{SiC} and ΔX_{SiC} represent the thermal conductivity, area and thickness of a presumed silicon-carbide interlayer between the growing diamond crystallite and the silicon substrate. T_{Di}, ε_{Di} and A_{Di} are the diamond crystal temperature, emissivity and surface area respectively, T_S is the temperature of the silicon substrate and σ, the Stephan-Boltzmann constant. In the above equation, Q_{conv} represents the convective heat flux from the gas stream and is approximated to first order by the product of the heat of combustion, the volumetric flow rate of acetylene, and the surface area of the substrate in contact with the flame. When the contact area between the diamond and underlying silicon is comparable to the surface area of the crystal, then the temperature difference is determined primarily by the contact thermal resistance. When the surface area of the growing crystal increases to the extent that

$$\frac{A_{Di}}{A_{SiC}} \gg \frac{k_{SiC} (T_{Di} - T_S)}{Q_{conv} \Delta X_{SiC}}$$

then the crystal can be taken as isolated, and its surface temperature is determined by the balance between conduction from the flame and radiation. We estimate the net heat flux from the gas phase onto the silicon surface to be on the order of 1 kW/cm^2. If the heat flux incident on the diamond face is comparable to this, then an isolated crystal would establish a surface temperature of approximately 1200 °C. Such a high temperature has been shown to favor graphite nucleation and growth[18-20]. Albeit somewhat simplified, this model suggests that extended growth with high enthalpy sources such as premixed flames or thermal plasmas can only be achieved provided that a sufficient thermal sink is established to prevent the growing crystals from reaching surface temperatures in excess of that which promote graphitic growth. For a continuous polycrystalline film, this means sufficient heat transfer between grains down to the water cooled substrate must be established.

IV. DISCUSSION

A. Flame Kinetics

A one dimensional flame kinetics model can be useful in understanding the temporal evolution of the gas phase chemistry within a volume element of premixed fuel travelling along a streamline from the torch nozzle. Such models have been frequently employed in the combustion community to describe quantitatively the structure of premixed flames when transport processes are negligible. In our case, such a model is at best qualitative downstream, at distances greater than the nozzle diameter, and is

obviously inapplicable in describing the chemistry within the secondary flame sheet. Nonetheless, it does provide some insight as to the composition of the post-primary flame zone approaching the diffusion boundary, which in essence represents a diluted fuel reacting with oxygen diffusing in from the surrounding ambient atmosphere.

We have employed CHEMKIN[21], which is a standard flame kinetics calculation package which solves the coupled species and energy conservation equations when a temperature-time history is specified. The elementary reaction set used is one that has been successful in predicting the chemistry of methane-air flames[22,23]. The temperature profile used is assumed to rise linearly with time from an initial temperature T_o (1200 K) to a maximum temperature T_m (3300 K) within 1 ms. These values are typical for oxyacetylene flames and the computed mole fractions within the post primary flame are not found to be extremely sensitive to these values. Results of the calculation for the major flame species and R = 0.8 are illustrated in Figure 11. As expected, the oxygen and acetylene mole fractions drop sharply, defining the primary flame front. The acetylene reaches a plateau signifying the full consumption of the oxygen. Based on a visual estimate of the length of the post primary flame zone and primary flame cone, and assuming negligible acceleration of the flow, then the volume element in question would encounter the diffusion flame zone within 0.2 - 0.4 ms. The results of the model calculations at t = 0.3 ms (see Table I), suggest that atomic hydrogen can be present at significant mole fractions, and should be the dominant radical species in the post primary flame zone. The atomic hydrogen should immediately attack molecular oxygen in the diffusion boundary via the three body reaction: $O_2\ (diff) + H + M \rightarrow OH + O + M$, sharply increasing both the OH and O radical mole fractions within the diffusion flame. The molecular oxygen mole fraction should drop in response, and a maximum C_2H mole fraction is likely to be established by a balance between acetylene oxidation:

$$C_2H_2 + O \rightarrow C_2H + OH$$

and subsequent oxidation of ethynyl:

$$C_2H + O \rightarrow CO + CH\ .$$

$$C_2H + OH \rightarrow HCCO + H\ .$$

The last reaction acts to replenish the atomic hydrogen radical pool.

The width of the diffusion flame region will be determined by the relative oxygen diffusion to chemical reaction rates. The absence of a narrow diffusion flame sheet as supported by the planar laser-induced fluorescence suggests that oxygen diffusion rate is comparable to its reactivity. This is expected since the remaining fuel within the post-primary flame zone is heavily diluted with combustion reaction products. These observations and computations have led us to believe that a more uniform deposit over

larger areas can be achieved by appropriate dilution of the fuel mixture with a noble gas such as argon. In addition, the role of the primary flame is simply to add heat and diluent to the reacting post primary gas stream. We emphasize here that the post primary gas stream *does not* directly participate in diamond growth in that the region of the surface in contact with this gas stream is found to contain non-diamond carbon. As we have discussed earlier, the high enthalpy gas stream may present a problem in terms of overheating the growing surface as well as in providing adequate cooling for more complicated substrate shapes. We therefore propose to use, and have begun experiments with a multi-nozzle *diffusion* flame. Such an approach permits better control of fuel dilution, is more fuel efficient, safer to operate with hydrogen addition and will circumvent the excessive heat load encountered with the premixed oxyacetylene flame. The results of that work will be presented in a future publication.

B. Implications on Growth Mechanism and Graphite Etching

The higher growth rates and improved diamond quality found in the region of the substrate in contact with the diffusion flame suggests that radicals other than atomic hydrogen and acetylene may play important roles in the flame synthesis of diamond. This is still within the framework of the model proposed by Frenklach and co-workers[8], however, the addition of the C_2H radical in the (111) diamond plane propagation (as an alternative to the C_2H_2 monomer proposed) might proceed without the need for hydrogen extraction, which has been shown to have an appreciable energy barrier[9]. Such a conjecture however, remains to be supported by quantum mechanical calculations.

The role of the OH and O radical, expected to be present in substantial quantities and in mole fractions greater than that of atomic hydrogen within the secondary flame zone needs to be investigated further. It is generally accepted that oxygen addition to the gas feed in most diamond deposition strategies lead to improved morphology and possibly growth rates. It has been recently suggested by Frenklach[24], that oxygen suppresses the formation of aromatic hydrocarbons in the gas phase which may condense to form a non-diamond deposit. More importantly, there is a great accumulation of data[25] that suggests that the graphite etching capability of atomic oxygen and OH can be two to three orders of magnitude greater than that of atomic hydrogen. This is particularly so at lower temperatures, and oxygen addition in any diamond growth strategy may eventually permit the room temperature growth of high quality diamond.

ACKNOWLEDGEMENTS

This work was supported in part by the Office of Naval Research. The authors wish to thank R. K. Hanson for use of the laser facility and G. Reynolds for the Raman spectra and SEM analysis.

REFERENCES

1. Karl E. Spear, J. Am. Ceram. Soc. **72**, 171 (1989).

2. Y. Hirose and Y. Terasawa, Japan. J. Appl. Phys. **2**, L519 (1986).

3. S. Matsumoto, Extended Abstracts from the 1988 Spring Meeting of the Materials Research Society, April 5-9, Reno Nevada.

4. L. M. Hanssen, W. A. Carrington, D. Oakes, J. E. Butler and K. A. Snail, Reprints of Papers Presented at the 197th ACS Meetings, Dallas, Texas, April 9-14, 1989.

5. L. M. Hanssen, W. A. Carrington, J. E. Butler and K. A. Snail, Mat. Lett. **7**, 289 (1988).

6. Y. Hirose and M. Mitsuizumi, New Diamond **4**, 34 (1988).

7. M. A. Stewart, J. A. Cooper, Jr. and W. A. Yarbrough, Book of Presentation Summaries, SDID/IST Diamond Technology Initiative Symposium, 11-13 July, 1989, Crystal City, VA.

8. M. Frenklach and K. E. Spear, J. Mat. Res. **3**, 133 (1988).

9. D. Huang, M. Frenklach and M. Maroncelli, J. Phys. Chem. **92**, 6379 (1988).

10. I. Glassmann, in *Combustion* (Academic, New York 1977), p. 50.

11. R. K. Hanson, J.Q.S.R.T. **40**, 343 (1988).

12. A. M. Wodtke and Y. T. Lee, J. Phys. Chem **89**, 4744 (1985).

13. W. M. Jackson, J. B. Halpern and C-S. Lin, Chem. Phys. Lett. **55**, 254 (1978).

14. J. R. McDonald, A. P. Baranovski and V. M. Donnelly, Chem. Phys. **33**, 161 (1978).

15. C. T. Bowman and D. J. Seery, Comb. Flame **12**, 611 (1968).

16. R. G. Joklik, J. W. Daily and W. J. Pitz, Proceedings, The 21st Symposium (International) on Combustion (The Combustion Institute), Pitt. PA (1986) p. 895.

17. Y. Mikada, Y. Kojima, T. Yoshida, K. Akashi, J. Mat. Sci. **22**, 1557 (1987).

18. S. Matsumoto, Y. Sato, M. Tsutsumi and N. Setaka, J. Mat. Sci. **17**, 3106 (1982).

19. A. Sawabe and T Inuzuka, Thin Solid Films **137**, 89 (1986).

20. Y. Saito, K. Sato, H. Tanaka, K. Fujita and S. Matuda, J. Mat. Sci. **23**, 842 (1988).

21. R. J. Kee, J. A. Miller and T. H. Jefferson, Sandia Report: SAND80-8003 UC-4, July (1987).

22. C. T. Bowman, private communication.

23. D. Seery and C. T. Bowman, Comb. Flame **14**, 37 (1970).

24. M. Frenklach and H. Wang. Book of Presentation Summaries, SDID/IST Diamond Technology Initiative Symposium, 11-13 July, 1989, Crystal City, VA.

25. D. E. Rosner, Annual Rev. Mat. Sci. **2**, 573 (1972).

FIGURE CAPTIONS

Fig. 1. Schematic of premixed oxyacetylene flame structure operating fuel rich.

Fig. 2. Laser based diagnostics facility for planar imaging of radicals within the secondary diffusion flame region.

Fig. 3. Pumping strategy for photodissociation fluorescence.

Fig. 4. Optical microscope images of flame deposit; a) after 5 minutes and; b) 15 minutes runs. The deposit is mostly in an annular region at early times with little carbon deposited in the center. Non-diamond carbon appears to nucleate in the central region during longer duration (>10 min.) runs. The quality of the diamond in the annular region also appears to deteriorate with longer duration runs.

Fig. 5. SEM analysis of a) central region and b) the annular region of 30 minute deposit.

Fig. 6. Micro-Raman analysis of the 30 minute deposit. The spot size of the laser beam is approximately 1 mm. The top spectrum is obtained from the outer (annular) region whereas the bottom spectrum is observed from the central region of the deposit.

Fig. 7. Planar laser-induced photodissociation fluorescence image of secondary diffusion zone. The image is believed to reflect the C_2H radical mole fraction (see text). The bright line serves to indicate the approximate location of the silicon surface.

Fig. 8. Histogram of the fluorescence signal parallel to and approximately 1 mm below the silicon substrate.

Fig. 9. Image of intrinsic 431 nm CH chemiluminescence. The bright line indicates the approximate location of the surface.

Fig. 10. Simplified thermal energy balance on growing crystallite.

Fig. 11. Results of the one-dimensional flame kinetics model for R = 0.8. The major species mole fractions are computed on the bases of the temperature profile given in text.

TABLE CAPTION

Table 1. Computed post-primary flame composition for R = 0.8, t = 0.3 ms, T(t) = 2200K. Only species with mole fractions in excess of 10^{-5} are listed.

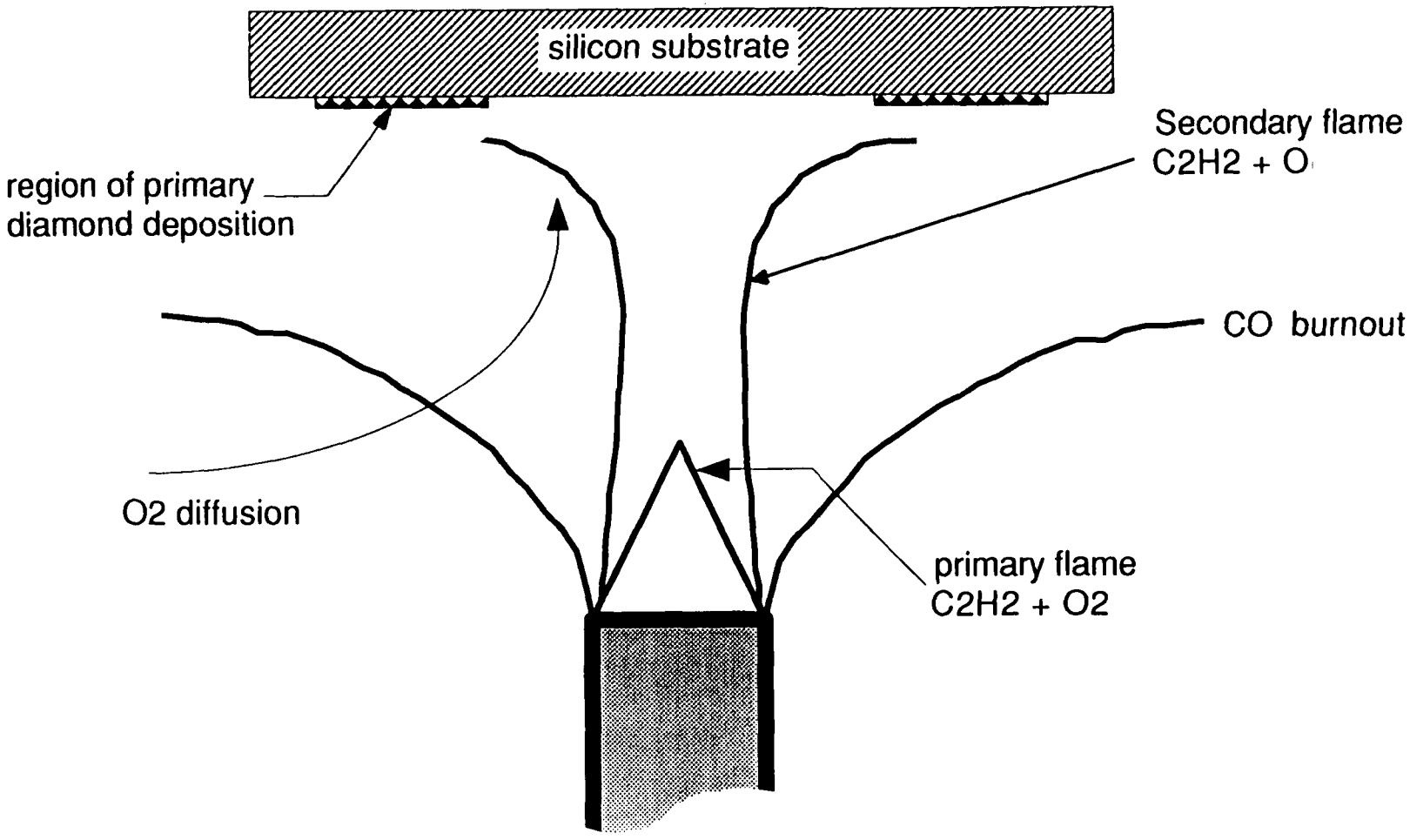
silicon substrate
region of primary
diamond deposition
Secondary flame
C2H2 + O
CO burnout
O2 diffusion
primary flame
C2H2 + O2

C2H2 / O2

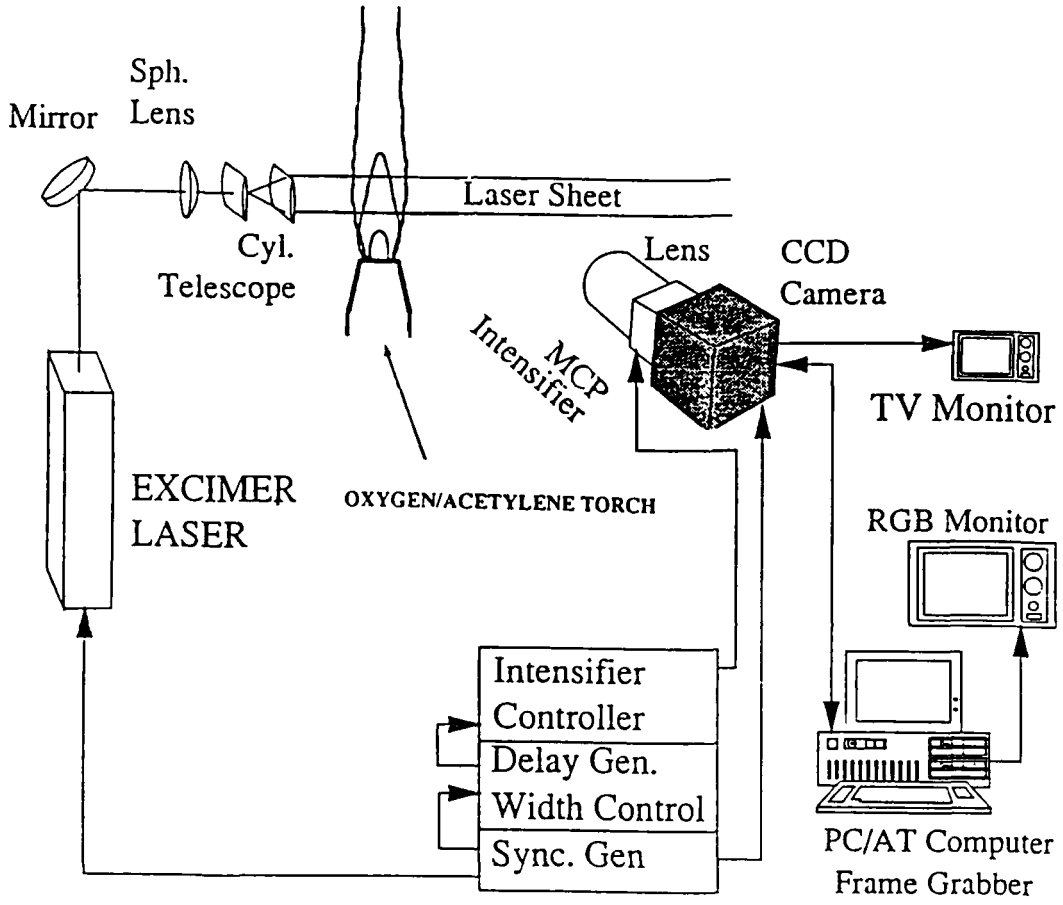
Sph.
Lens
Mirror
Laser Sheet
Cyl.
Telescope
Lens
CCD
Camera
MCP
Intensifier
TV Monitor
EXCIMER
LASER
OXYGEN/ACETYLENE TORCH
RGB Monitor
Intensifier
Controller
Delay Gen.
Width Control
Sync. Gen
PC/AT Computer
Frame Grabber

Figure 2

LASER INDUCED PHOTODISSOCIATION FLUORESCENCE of C_2H_2 and C_2H

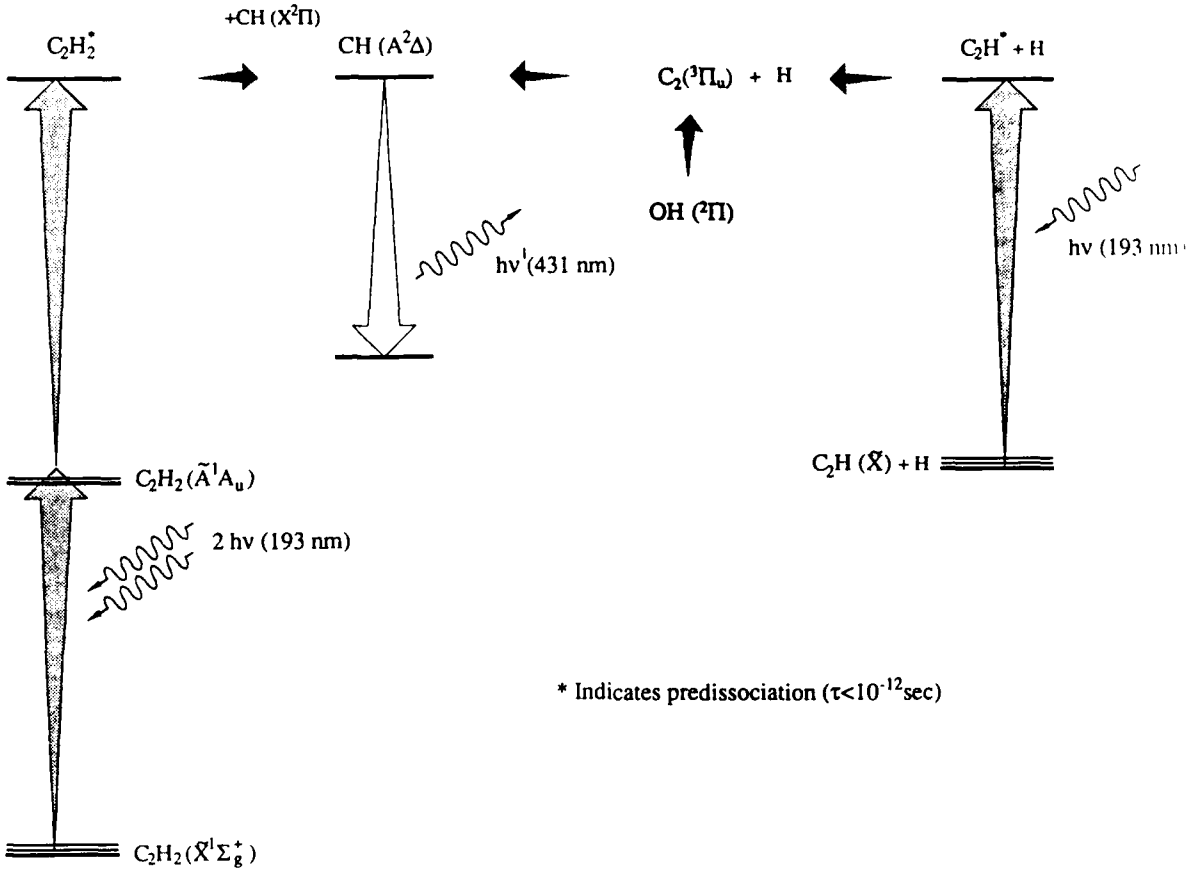

* Indicates predissociation ($\tau<10^{-12}$sec)

Figure 3

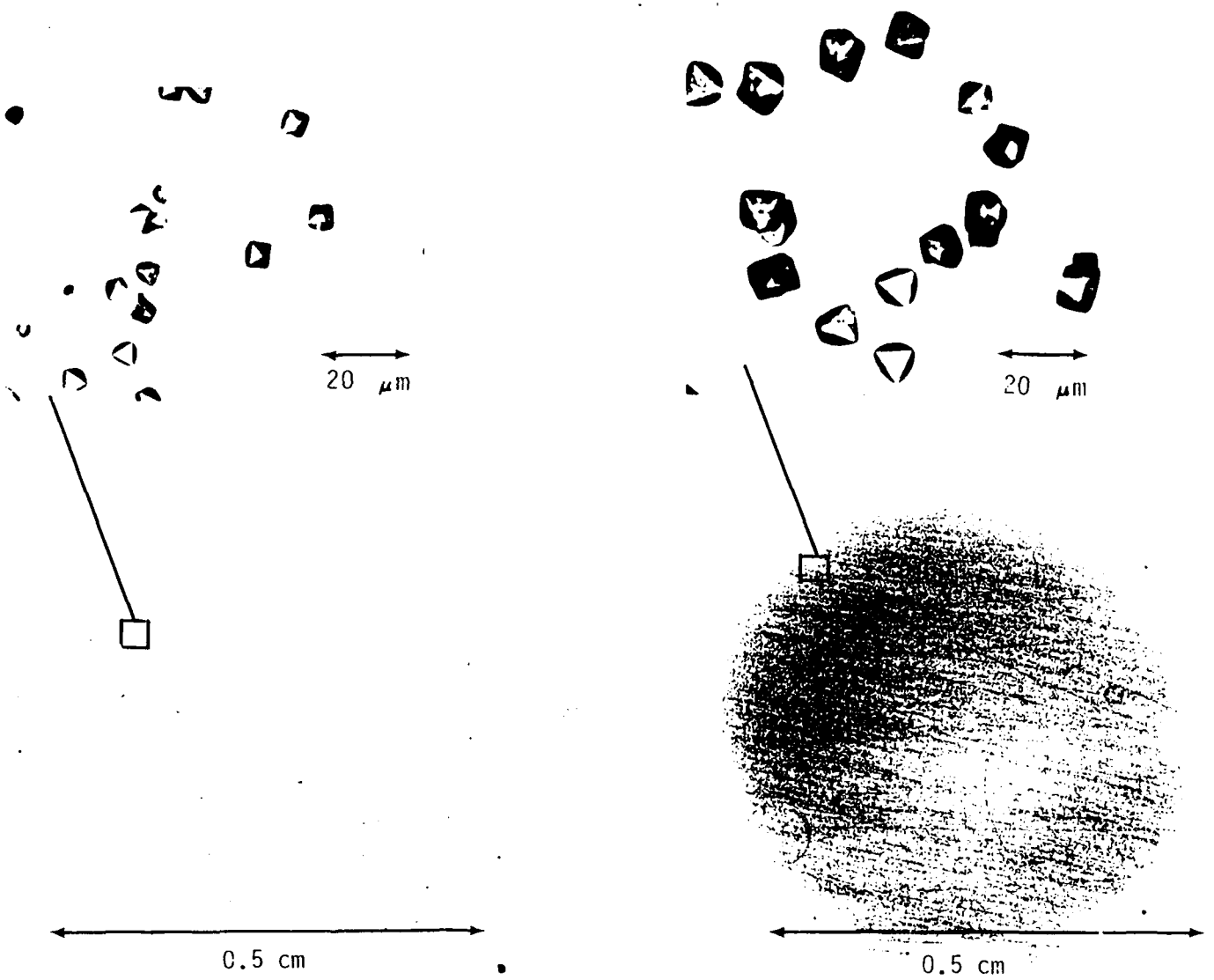

Figure 1

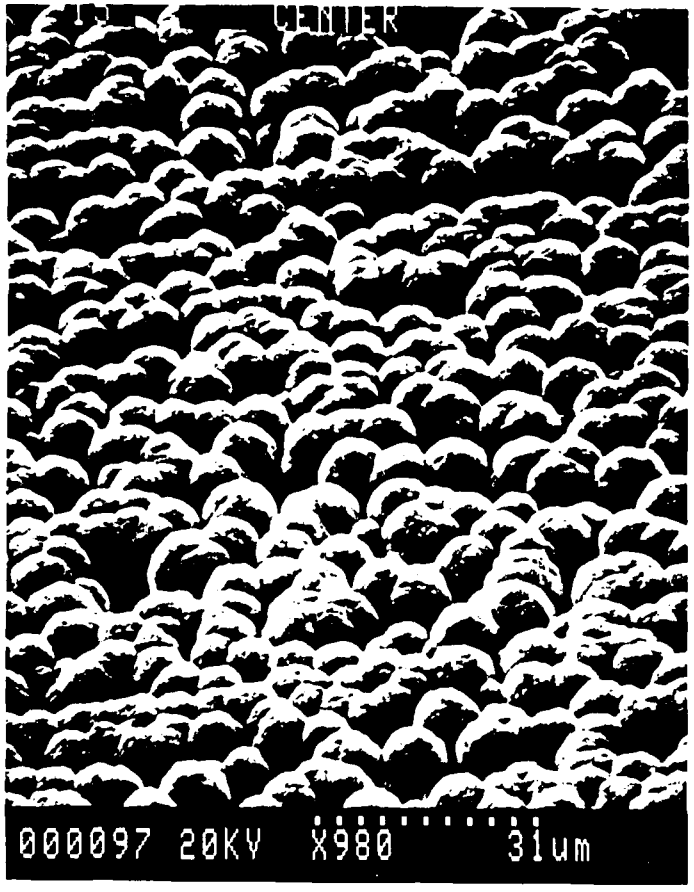
CENTER
000097 20KV X980 31um

a)


BORDER
CENTER/OFF CENTER
000099 20KV X2.16K 13.9um

b)

Figure 5

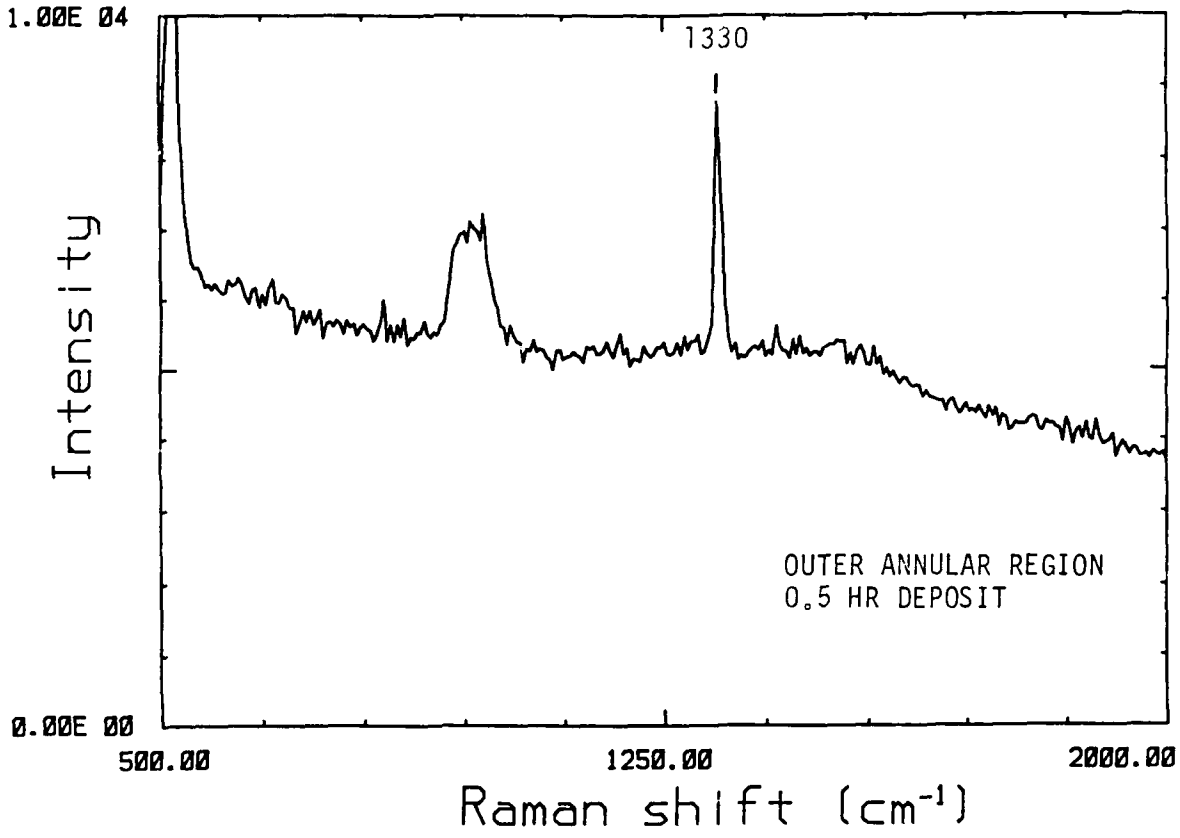
1.00E 04
1330
Intensity
OUTER ANNULAR REGION
0.5 HR DEPOSIT
0.00E 00
500.00
1250.00
2000.00
Raman shift (cm-1)

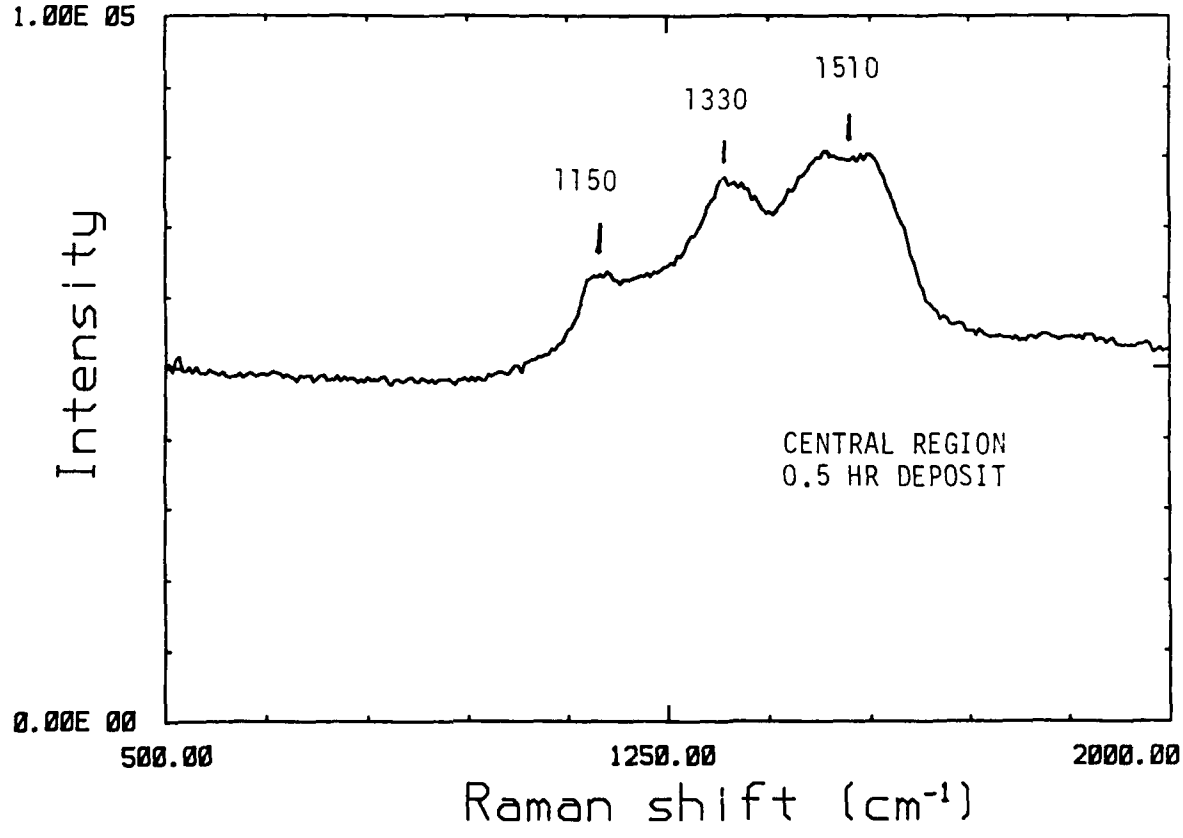
1.00E 05
1510
1330
1150
Intensity
CENTRAL REGION
0.5 HR DEPOSIT
0.00E 00
500.00
1250.00
2000.00
Raman shift (cm-1)

Figure 6

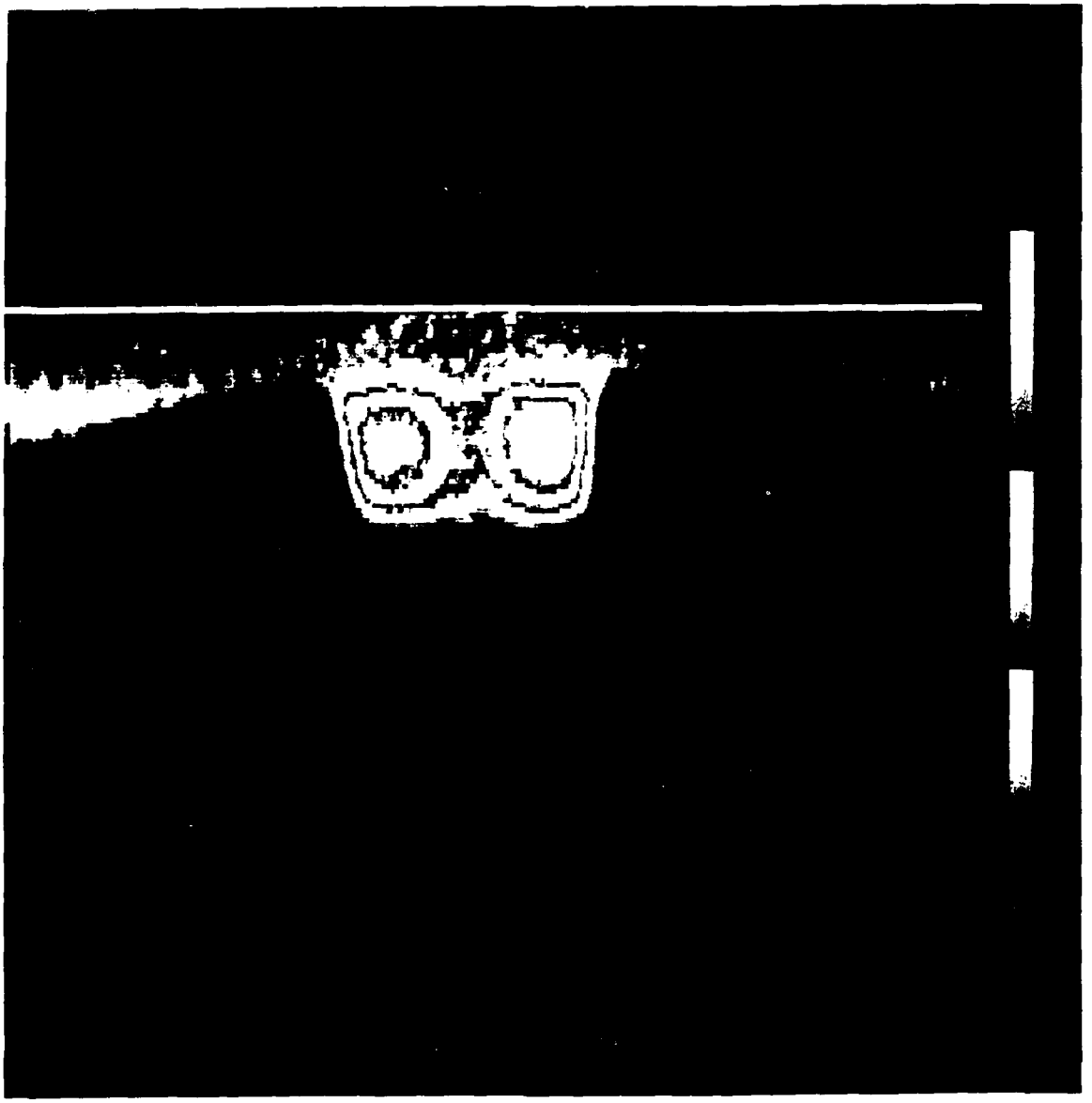

Figure 7

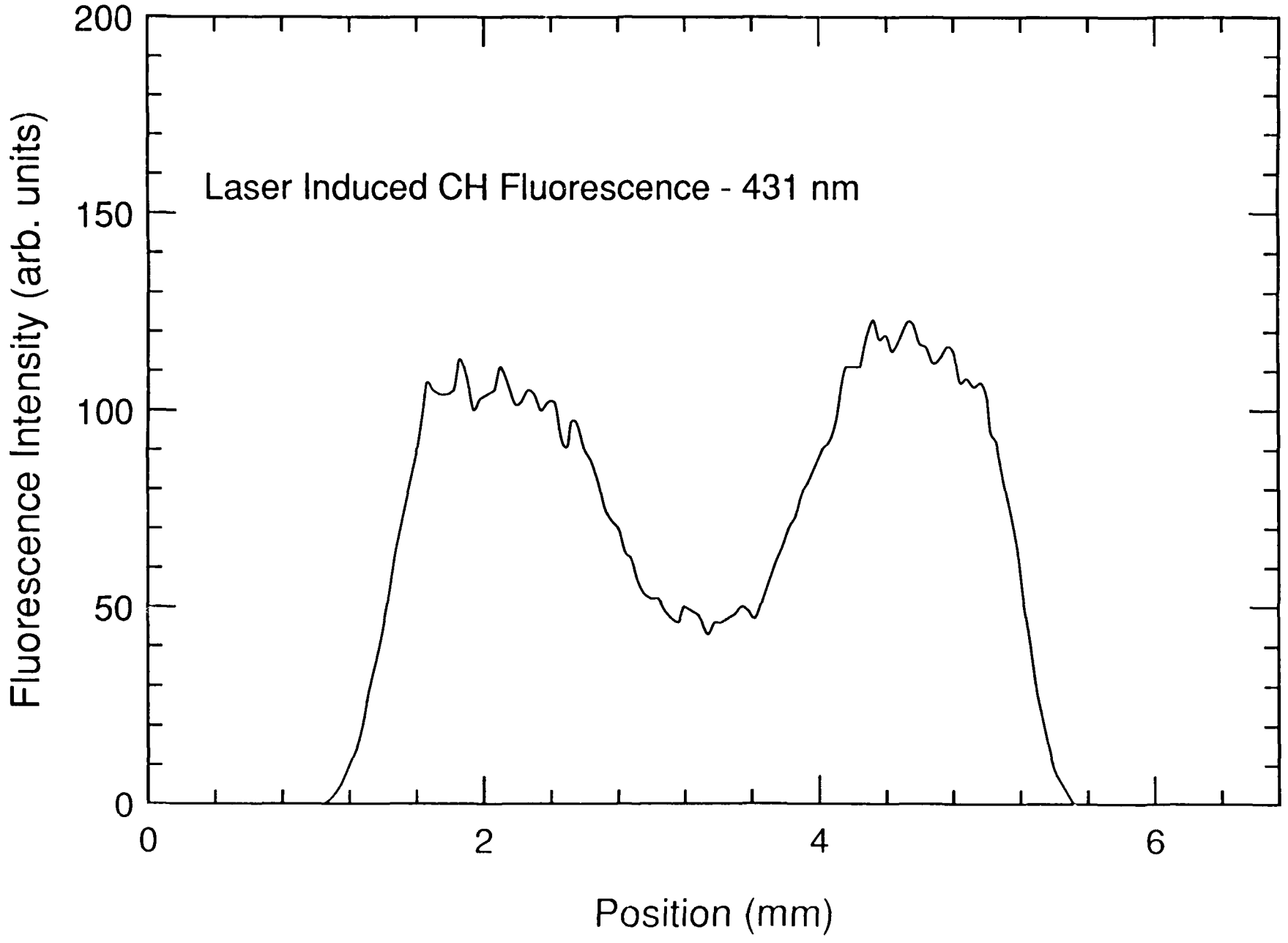
Laser Induced CH Fluorescence - 431 nm
Fluorescence Intensity (arb. units)
200
150
100
50
0
0
2
4
6
Position (mm)

figure 8

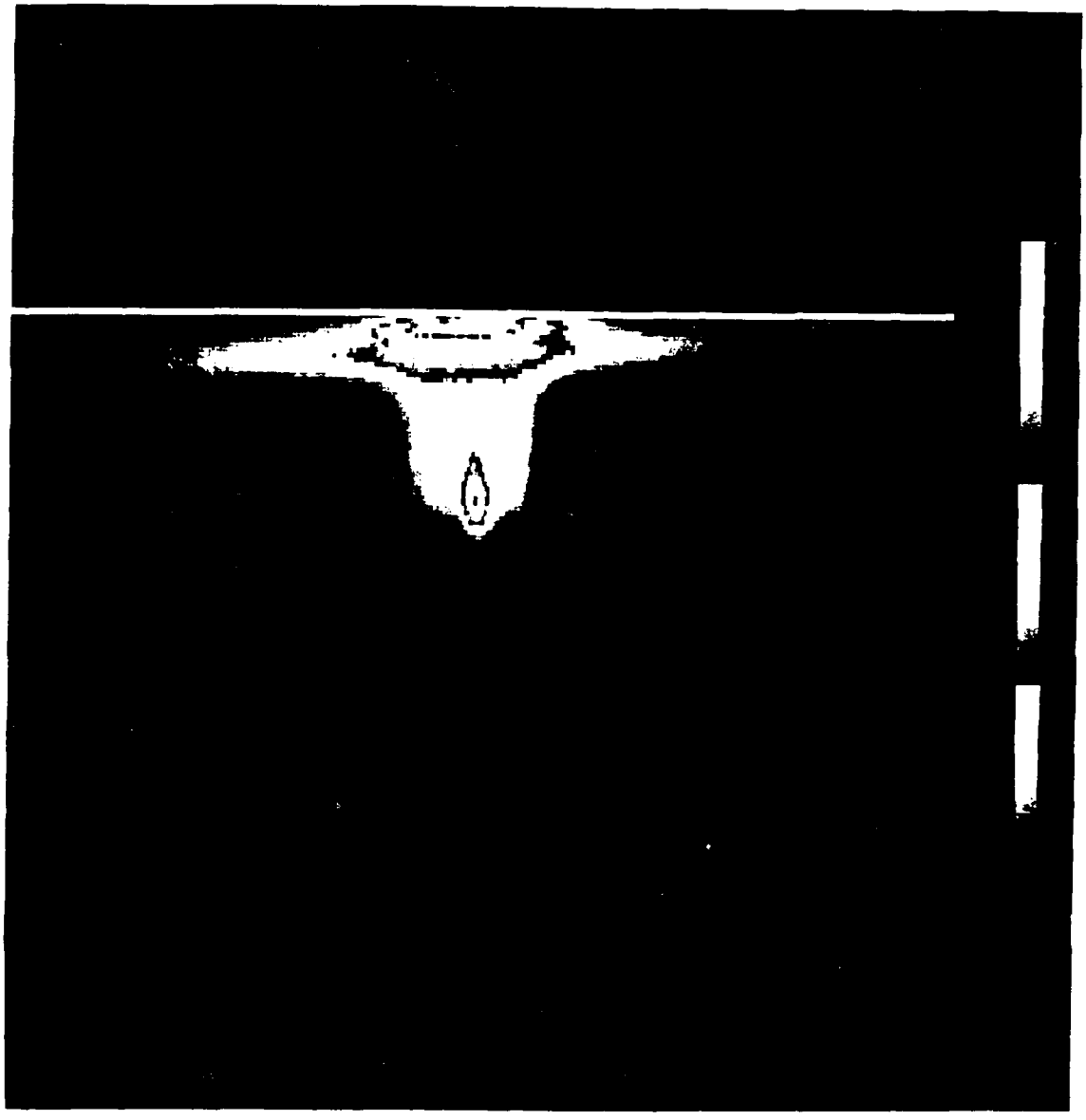

Figure 9

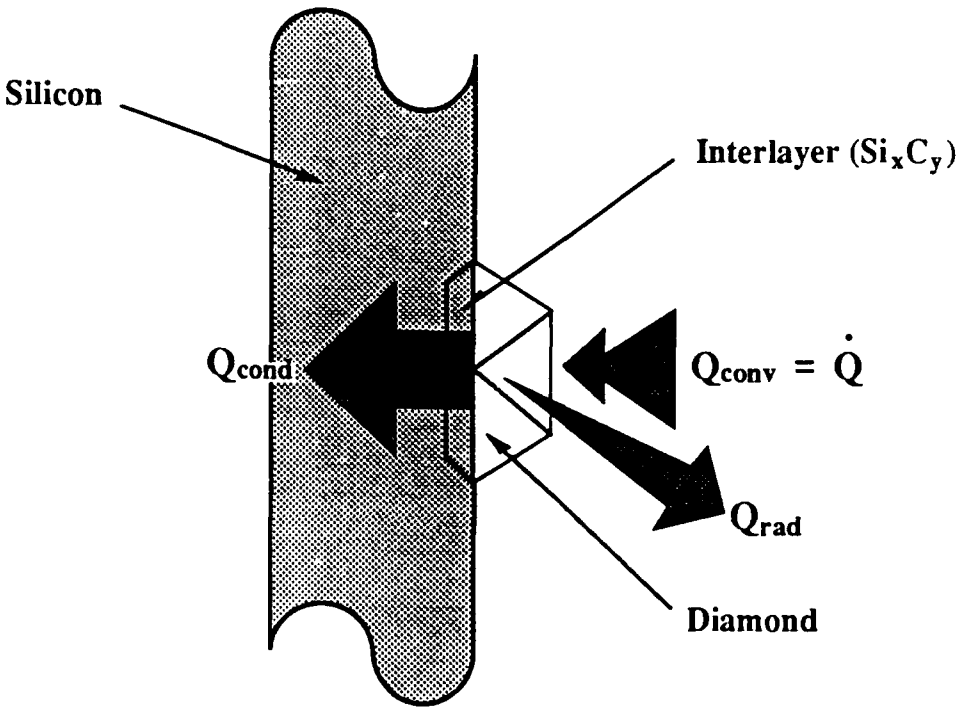

Figure 10

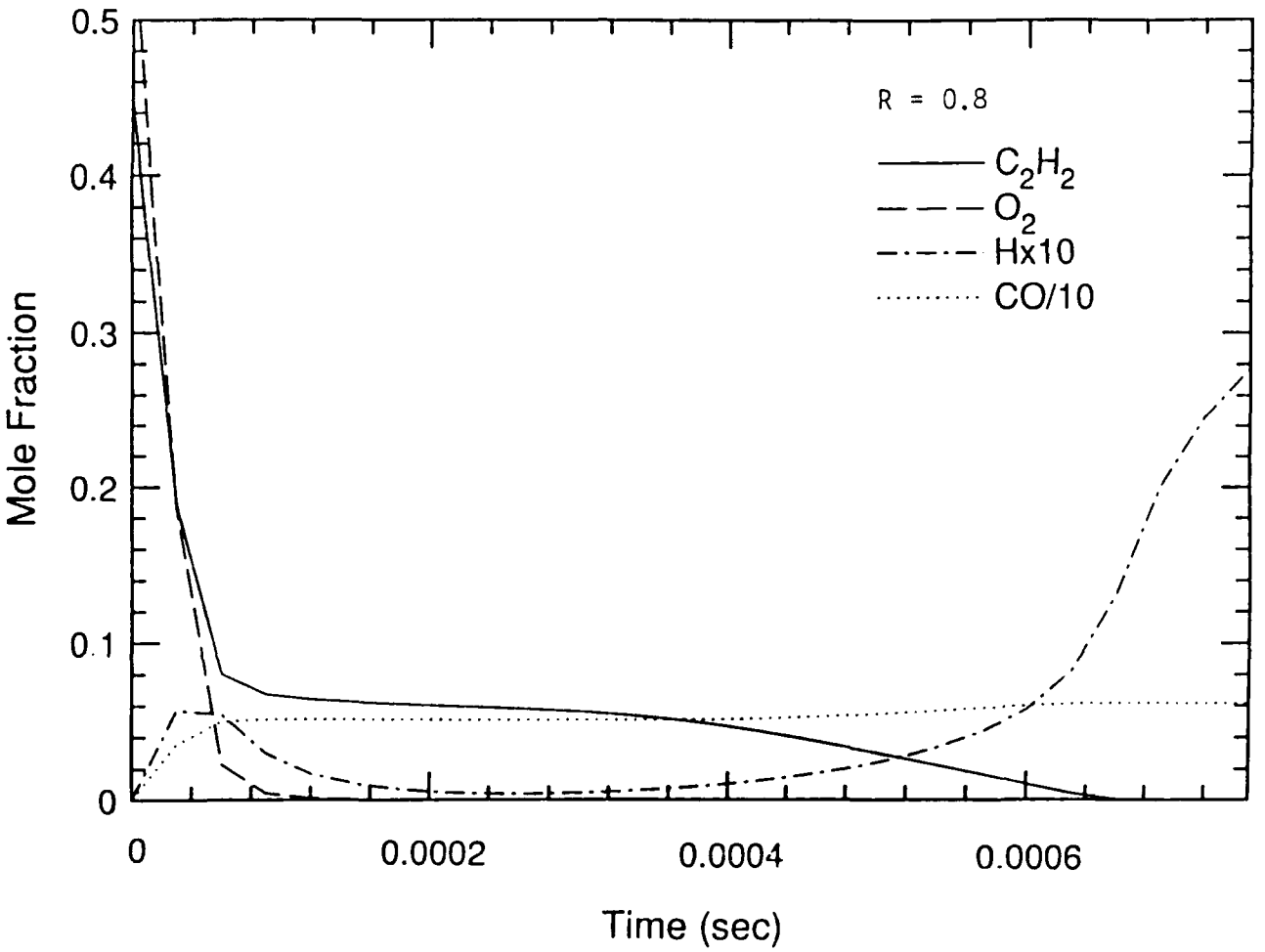
R = 0.8
C_2H_2
O_2
Hx10
CO/10
Mole Fraction
0.5
0.4
0.3
0.2
0.1
0
0
0.0002
0.0004
0.0006
Time (sec)

Figure 11

Species	Mole Fraction
CO	0.509
H_2O	0.1828
H_2	0.1263
CO_2	0 1164
C_2H_2	0.0562
CH_4	3.69×10^{-3}
C_4H_2	1.90×10^{-3}
C_3H_2	1.70×10^{-3}
H	4.56×10^{-4}
CH_3	3.3×10^{-4}
C_3H_3	2.8×10^{-4}
C_2H_4	2.3×10^{-4}
HCCO	1.7×10^{-4}
OH	8.8×10^{-5}

Table 1

IR DOMES DISTRIBUTION LIST

October 1988

Dr. W. Adler
General Research Inc.
P. O. Box 6770
Santa Barbara, CA 93160

R. A. Heinecke
Standard Telecommunication
Laboratories, Ltd.
London Road
Harlow, Essex CM17 9MA
England

Mr. D. Roy
Coors Porcelain Co.
Golden, CO 80401

Dr. Mufit Akinc
Mat'ls Science & Eng. Dept.
Iowa State University
110 Engineering Annex
Ames, IA 50011

Dr. Lisa C. Klein
Center for Ceramics Research
College of Engineering
Rutgers University
P. O. Box 909
Piscataway, NJ 08854

Dr. D. Roy
Mat'ls Science Lab
Pennsylvania State Univ.
University Park, PA 16802

Dr. H. E. Bennett
Code 38101
Naval Weapons Center
China Lake, CA 93555

Dr. P. Klocek
Texas Instruments
P. O. Box 660246
Dallas, TX 75266

Dr. J. Savage
Royal Signals & Radar Establishment
St. Andrews Road
Great Malvern, WORCS, WR14 3PS
ENGLAND

Dr. S. Block
Group Leader
Structural Chemistry
National Bureau of Standards
Gaithersburg, MD 20899

Dr. R. Messier
Pennsylvania State University
Materials Research Lab
University Park, PA 16802

Dr. A. Stacy
Chemistry Departament
Univ. of Calif. Berkeley
Berkeley, CA 94720

Dr. J. Burdett
Chemistry Department
University of Chicago
Chicago, IL 60637

Dr. G. Messing
Materials Research Department
Pennsylvania State University
University Park, PA 16802
(1 copy for distribution)

Dr. I. G. Talmy, Code R31
Naval Surface Weapons Center
White Oak Laboratory
Silver Spring, MD 20903

Dr. Mark A. Cappelli
Mechanical Engineering Dept.
Stanford University
Stanford, CA 94305

Dr. S. Musikant
General Electric Company
P. O. Box 8555
Philadelphia, PA 19101

Dr. R. Tustison
Raytheon Co., Research Div.
131 Spring Street
Lexington, MA 02173

Dr. J. A. Cox
Honeywell Systems & Research
Dept. MN 65-2600
3660 Technology Drive
Minneapolis, MN 55418

Dr. Dale Perry
U.S. Army Missile Command
Redstone Arsenal
Huntsville, AL 35807

Dr. W. White
Materials Research Lab
Pennsylvania State Univ.
University Park, PA 16802

Dr. B. Dunn
Materials Science & Eng. Dept.
Univ. of California, Los Angeles
Los Angeles, CA 90024

Dr. W. Pittman
AMSI-RD-AS-PM
Redstone Arsenal
Huntsville, AL 35898

Dr. A. Wold
Chemistry Department
Brown University
Providence, RI 02912

Naval Surface Weapons Ctr
10901 New Hampshire Ave
White Oak Laboratory

Dr. A. Harker
Rockwell International
P. O. Box 1085
1049 Camino Dos Rios
Thousand Oaks, CA 91360

Dr. R. Raj
Materials Science&Eng. Dept.
Cornell University
Ithaca, NY 14853

Capt. Ken L. Yates
AD/AFATL/AGA
Eglin AFB, FL 32542

Office of Naval Research
800 N. Quincy Street
Arlington, VA 22217
Attn:Code1113(H.Guard)
" " " " " " " " "(D.Nelson)

Dr. D. C. Harris (Code 3854)
Naval Weapons Center
China Lake, CA 93555
(1 copy for distribution)

Dr. W. Rhodes
GTE Laboratories
40 Sylvan Road
Waltham, MA 02134

Defense Documentation Center
Cameron Station
Alexandria, VA 22314
(12)

Dr. R. W. Schwartz
Code 38504
Naval Weapons Center
China Lake, CA 93555

Naval Air Systems Cmd
1411 Jeff Davis Hwy.
Arlington, VA 22202
Attn:Code 931A (L.Sloter)

Scientific Advisor
Commandant of the
MarineCorps(CodeAX)
Washington,DC 20380

Office of Naval Technology
800 N. Quincy Street
Arlington, VA 22217
Attn:Code 0712(1) Code 0725 (1)